J Mater Sci (2022) 57:12405–12415

Chemical routes to materials

Ball-milling-assisted solid-state synthesis of $Mn_yCe_{1-y}O_x$ catalysts for 1, 2-dichlorobenzene destruction at low temperature

Shengyong Lu[1], Xuanhao Guo[1], Yumeng Gu[1], Yaqi Peng[1,*], Jiamin Ding[1], and Jianhua Yan[1]

[1] State Key Laboratory of Clean Energy Utilization, Institute for Thermal Power Engineering, Zhejiang University, Hangzhou 310027, China

Received: 14 March 2022
Accepted: 9 June 2022
Published online: 30 June 2022

ABSTRACT

A series of Mn–Ce composite oxides catalysts ($Mn_yCe_{1-y}O_x$) prepared by co-precipitation method and ball-milling-assisted solid-state synthesis were tested for the catalytic combustion of 1,2-dichlorobenzene. The results showed that ball milling process as a green chemistry method can significantly promote the catalytic activity. The Mn/Mn + Ce ratio also has an important influence on the degradation of dichlorobenzene. Complete combustion of 1,2-dichlorobenzene is achieved on $Mn_{0.85}Ce_{0.15}O_x$ at 193 °C, which is much lower than the catalysts reported in the references. Characterization by BET, HRTEM, XRD, XPS, H_2-TPR and NH_3-TPD revealed that the high activity at low temperature was attributed to the advantages of the formation of Mn–O–Ce solid solution, abundant surface-active oxygen, and developed pore structure induced by ball milling synthesis. The current work provides the potential to use the ball-milling-assisted solid-state synthesis as a green chemistry method for catalytic destruction of persistent organic pollutants.

Introduction

In recent years, the emission control of dioxins in flue gas from municipal solid waste incineration has attracted much attention due to the increased output of solid waste and the increasingly strict emission standard[1]. Dioxins as toxic substances have the characteristics of persistence, biological accumulation and long-distance migration, highly harmful to the environment[2]. Therefore, it is of great significance to effectively control the generation and diffusion of dioxins. Among the control technologies [3], catalytic combustion has been proved to be a promising technology for the removal of dioxin-like substances due to its low-temperature conversion and high selectivity[4, 5].

Handling Editor: Pedro Camargo.

Address correspondence to E-mail: pengyaqi@zju.edu.cn

https://doi.org/10.1007/s10853-022-07426-y

Cerium oxides has gained increasing attention in the catalytic degradation of chlorine-containing volatile organic pollutants in recent years due to the excellent oxygen storage-release capabilities[6]. When used to catalyze the degradation of chlorinated aromatic pollutants, the CeO_2 catalyst will be deactivated quickly. The interaction between CeO_2 and Cl is vigorous when the temperature is below 400 °C, and Cl will accumulate on the surface of the catalyst[7]. Therefore, if the Cl on the catalyst surface can be removed in time, the stability of the CeO_2 catalyst can be greatly improved. It is well known that the doping of transition metal, precious metal or rare earth metal can improve the catalytic activity and stability of CeO_2-based catalysts. Among the commonly used metal additives, e.g., Pt[8], W[9], V[10], Ti, Cu[11, 12] and Mn[13], the combined oxides of Mn and Ce showed the best catalytic performance in the degradation of chlorobenzene. This is mainly attributed to the formation of Mn–O–Ce solid solution structure with rich oxygen content and strong reductive Mn^{4+}[13].

So far, $Mn_yCe_{1-y}O_x$ catalysts have been widely prepared for the degradation of chlorobenzene by the impregnation method, sol-gel method, and co-precipitation method[14, 15]. However, these traditional preparation methods are complicated and use many solvents in the preparation process. In recent years, the preparation of heterogeneous catalysts by ball milling has attracted wide attention because of its simple operation, low cost, and no solvent consumption[16]. The ball-milling-assisted preparation of transition metal oxide catalysts for the catalytic degradation of chlorobenzene attracted much attention, and it has been demonstrated that the ball-milling samples showed encouraging activity as compared to their sol-gel analogues[17]. However, few studies are reported on exploring the behavior of mechanically assisted synthesis of $Mn_yCe_{1-y}O_x$ mixed oxide catalysts in the oxidation of chlorinated volatile organic compounds.

In this study, a series of $Mn_yCe_{1-y}O_x$ catalysts were prepared using ball-milling-assisted solid-state synthesis with different molar ratios of Mn/Ce + Mn. The $Mn_yCe_{1-y}O_x$ mixed oxide catalysts were tested in catalytic combustion of 1,2-dichlorobenzene, and the effects of preparation methods and Mn amount were investigated. Moreover, combining the BET, HRTEM, XPS, XRD, H_2-TPR, and NH3-TPD characterization data, the influences of Mn–O–Ce solid solution structure, redox capacity, and acidity on catalysts activity were discussed.

Materials and methods

Catalyst preparation

As shown in Scheme 1, $Mn_yCe_{1-y}O_x$ catalysts were prepared by the ball milling and calcination synthesis. A total of 15 g $Ce(NO_3)_3$•$6H_2O$ and $Mn(NO_3)_2$•$4H_2O$ were put in a zirconia ball milling tank (250 ml) with zirconia spheres (total mass 375 g, diameter 10 mm and 5 mm, mass ratio 1:1). Then, the tanks were placed in a planetary ball mill (QXQM-2-DW, Changsha Tianchuang, China). The rotation speed of the planetary disk was set as 500 rpm and the duration of 2 h. Finally, the $Mn_yCe_{1-y}O_x$ catalysts powder were obtained by calcining in the Muffle furnace at 400 °C for 3 h in the air atmosphere. The Mn/Mn + Ce ratio was 0, 0.25, 0.5, 0.75, 0.85, and 1, respectively, and the catalysts were denoted as MnCeO-BM. All the obtained powder catalysts were sieved to catalyst pellets in sizes of 0.2–0.4 mm.

$MnCeO_x$ catalysts with the same composition as mentioned above were also synthesized by a traditional co-precipitation method and denoted as MnCeO-CP.

Catalyst characterization

The specific surface areas and pore structure of the catalysts were determined using N_2 adsorption–desorption isotherms measured at − 196 °C using a Micromeritics Tristar II 3020 version 3.02 analyzer. The specific surface areas were calculated from the isotherms using the Brunauer–Emmett–Teller (BET) method. The pore size distribution was obtained using the Barrett–Joyner–Halenda (BJH) method.

High-resolution transmission electron microscopy (HRTEM) images of the as-prepared catalysts were acquired on a 120-kV transmission electron microscope (HT-7700, Hitachi). The powder X-ray diffraction patterns (XRD) of samples were recorded on a Rigakuultimaiv of Neo-Confucianism powder diffractometer using Cu Kα radiation (40 kV and 40 mA). The diffractograms were recorded in the 2θ range of 10–80° with a 2θ step of 2°/min. The X-ray photoelectron spectroscopy (XPS) measurements were made on a ThermoScientificK-Alpha

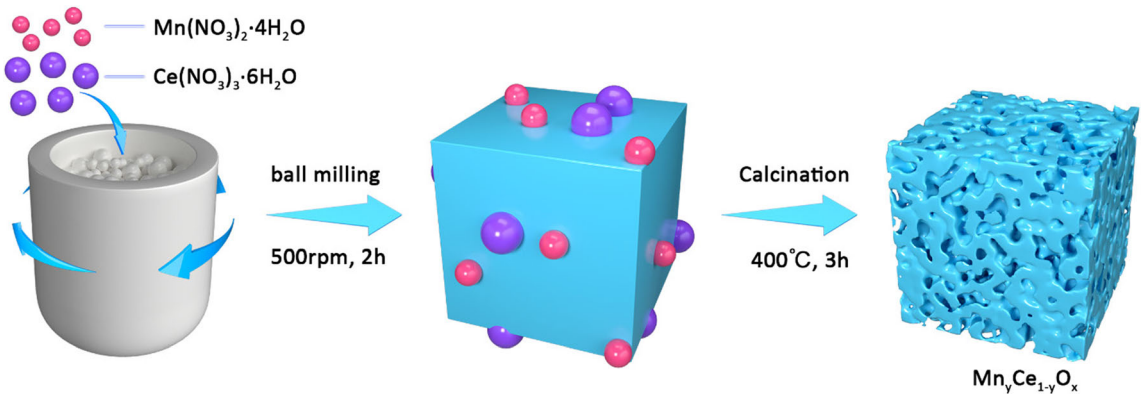

Scheme 1 Schematic diagram for preparing MnyCe1-yOx catalysts by ball milling synthesis.

spectrometer by using Mg Kα (1253.6 eV) radiation as the excitation source. The charging of samples was corrected by setting the binding energy of adventitious carbon (C1s) at 284.6 eV. H_2-TPR is used to determine the surface reducibility of the catalyst. NH_3-TPD was conducted in Micromeritics AutoChem II 2920 apparatus equipped with a TCD detector to determine the surface acidity of the catalyst. The total concentrations of various elements (Mn and Ce) in each catalyst sample were obtained by inductively coupled plasma optical emission spectrometry (ICP-OES) analysis, which was performed on a Agilent 5110 (Agilent, America).

Catalytic performance evaluation

1,2-Dichlorobenzene, as a chlorinated volatile organic pollutant, is a commonly used experimental model when studying catalysts for the degradation of dioxin [18–20]. In this study, the bubbling method is used to generate a stable source of 1,2-dichlorobenzene with an initial concentration of 117 ppm. The catalytic reaction part of the experimental system consists of a quartz tube reactor with an inner diameter of 8 mm and a tube furnace. The 1,2-dichlorobenzene catalytic reaction temperature is set in the range of 150–350 °C, controlled by the temperature controller. The total flow of reaction gas is 200 ml/min, and the space velocity is 15,000 h^{-1}. The concentration of dichlorobenzene in the flue gas was determined by an online gas chromatograph (Fuli 7890A, China). The surface of the gas pipeline was kept at 120 °C with heating tape in case of condensation loss.

The conversion efficiency of the catalysts to 1,2-dichlorobenzene was calculated by the following formula, C_{inlet} is the concentration of 1,2-dichlorobenzene, and C_{outlet} is the concentration of 1,2-dichlorobenzene in the tail gas:

$$\eta_{DCBz} = \frac{C_{inlet} - C_{outlet}}{C_{inlet}} \times 100\% \quad (1)$$

Results and discussion

Composition and structure

The N_2 adsorption–desorption isotherms of the catalysts under ball-milling-assisted process and co-precipitation methods were typical type IV isotherms (IUPAC) as shown in Fig. 1a, indicating that the two catalysts studied are mesoporous materials. The presence of an H3 hysteresis ring indicates that the pore structure of the catalyst is a wedge-shaped pore formed by the loose accumulation of flake particles[21]. The textural properties of $Mn_yCe_{1-y}O_x$ catalysts are illustrated in Table 1. For the $Mn_{0.5}Ce_{0.5}O_x$-BM sample, its specific surface area is 86 m^2/g, which is higher than that of $Mn_{0.5}Ce_{0.5}O_x$-CP samples. The total pore volume of $Mn_{0.5}Ce_{0.5}$Ox-BM is 0.23 cm^3/g, twice that of $Mn_{0.5}Ce_{0.5}O_x$-CP catalysts (0.13 m^3/g). The pore size distributions for these two types of catalysts are displayed in Fig. 1b. It can be seen that the $Mn_{0.5}Ce_{0.5}O_x$-BM sample had a larger specific surface area and pore volume, which is mainly due to the mechanical action in the form of kinetic energy and friction heating, which may produce a high degree of interstitial porosity in the solid-state redox reaction.

Figure 2 shows TEM and HRTEM images of $Mn_{0.85}Ce_{0.15}O_x$ catalyst prepared by the ball milling synthesis. The catalyst exhibited a lamellar structure,

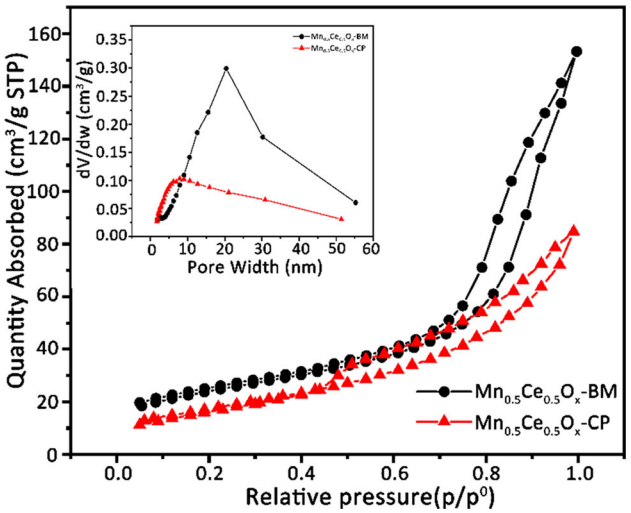

Figure 1 **a** N_2 adsorption–desorption isotherms of $Mn_{0.5}Ce_{0.5}O_x$-BM, $Mn_{0.5}Ce_{0.5}O_x$-CP; **b** the corresponding pore size distribution obtained from the adsorption branch.

and under high resolution TEM (Fig. 2b), the lattice spacing is measured to be 0.2986 nm, which is consistent with the (111) surface of face-centric (FCC) CeO_2 (0.3123 nm) but significantly lower than the theoretical value. This indicates that some Mn ions are bonded to the CeO_2 lattice, causing lattice contraction[17].

Figure 3 shows XRD patterns of $Mn_yCe_{1-y}O_x$ samples in the y range of 0–1 and $Mn_{0.5}Ce_{0.5}O_x$-CP samples. For the diffraction pattern of CeO_2, the characteristic diffraction peak of CeO_2 with face-centered-cubic (FCC) fluorite structure is observed. The characteristic reflections at 28.55, 33.08, 47.48, 56.35, 59.37, 69.45 and 76.7° correspond to the (111), (200), (220), (311), (222), (400) and (331) planes, respectively. When Mn is added, the $Mn_{0.25}Ce_{0.75}O_X$ catalyst sample has a similar diffractogram with the CeO_2 catalyst, but the peak intensity of the Ce phase decreases, indicating that Mn doping can inhibit CeO_2 crystallization. This is consistent with the conclusion of the lattice shrinkage as shown by the TEM characterization results, and it has been further confirmed in the remaining $Mn_yCe_{1-y}O_x$ samples. When the molar ratio of Mn/(Mn + Ce) is greater than 0.5, the CeO_2 diffraction peak at 28.5° gradually shifts to a higher value, indicating that the Mn species enter the Ce fluorite lattice and form a Mn–O–Ce solid solution[22]. For $Mn_{0.85}Ce_{0.15}O_x$, the obtained XRD pattern gradually resembles the diffraction pattern of MnOx. The diffraction peak corresponding to $Mn_{0.85}Ce_{0.15}O_X$ sample almost disappears, which may due to the high dispersion of Ce species in the MnOx matrix or just poor crystallinity. The former is more reliable because it was consistent with the high catalytic performance of $Mn_{0.85}Ce_{0.15}O_x$. Moreover, two small peaks appear at 32.9° and 37.2°, i.e.,α-Mn_2O_3[23] crystals in the form of dipyroxene and

Table 1 Textural Properties of $Mn_{0.5}Ce_{0.5}O_x$ Catalysts

Samples	S_{BET}[a] (m^2/g)	V_P[a] (cm^3/g)	D_a[a] (nm)	ICP-OES Mn/Ce(mol/mol)
$Mn_{0.5}Ce_{0.5}O_x$-BM	85.5	0.23	10.48	1.09
$Mn_{0.5}Ce_{0.5}O_x$-CP	63.53	0.13	7.94	1.1

[a] Structural parameter of the catalysts obtained by N_2 adsorption–desorption; SBET, BET surface area; Vp, total pore volume; Da, average pore diameter

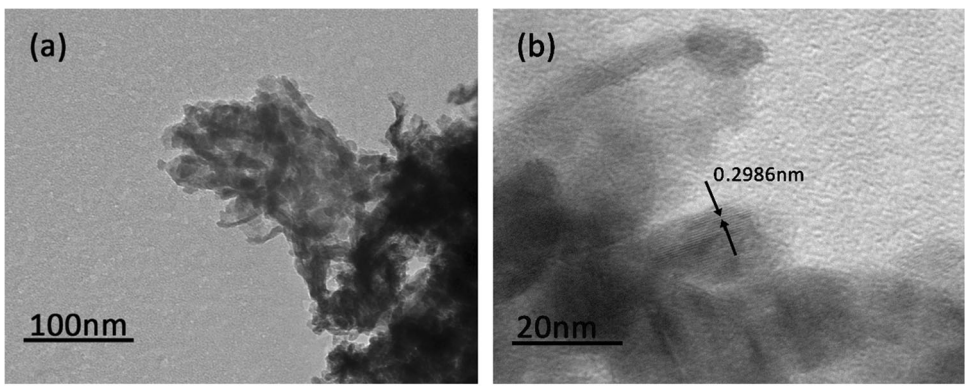

Figure 2 TEM **a** and HRTEM **b** images of the $Mn_{0.85}Ce_{0.15}O_x$-BM catalyst.

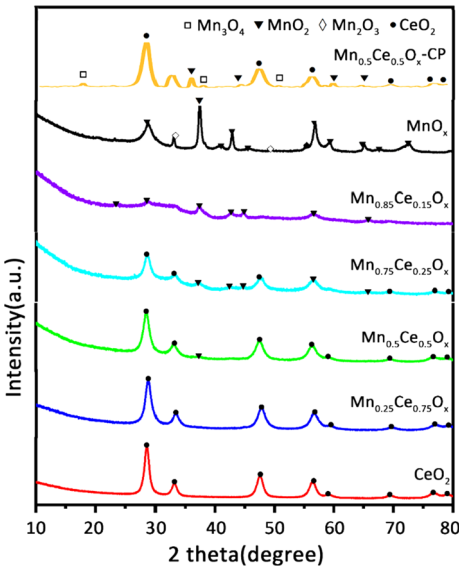

Figure 3 XRD patterns of the $Mn_yCe_{1-y}O_x$ catalysts with different Mn/(Mn + Ce) ratios.

MnO_2[24] crystals in the form of pyrosite. For pure MnOx, the reflection of α-Mn_2O_3 phase and MnO_2 phase occurs. $Mn_{0.5}Ce_{0.5}O_x$-CP samples showed higher diffraction peak intensity may be due to different preparation methods, and a few Mn_3O_4 phase was observed. In general, the XRD results once again confirm the formation of Mn–O-Ce solid solution structure by the ball-milling-assisted solid-state synthesis, which performs a significant effect on improving catalyst activity.

Figure 4a shows the O 1_S spectra, which are divided into three main bands. The three characteristic peaks are deconvoluted around 529.5, 531.3 and 533.5 eV, which correspond to lattice oxygen, adsorbed oxygen and weakly bonded oxygen species (active oxygen)[25, 26], respectively. The distribution ratio of oxygen species is shown in Table 2. With the addition of Mn, the binding energy of O1s of lattice oxygen on $Mn_yCe_{1-y}O_x$ catalysts shifts from 529.4 to 529.8 eV with the "O→Mn" electron transfer process, and the amount of lattice oxygen is reduced[27]. With the increase in Mn/(Mn + Ce) ratio from 0.25 to 0.85, the binding energy position of oxygen adsorption on the surface at 531.3 eV does not change with the increase in Mn content, but the content of reactive oxygen increases from 36.5 to 48%. The data improvement of O_{sur}/O_{all} indicates that the surface-active oxygen increases, which greatly promotes the oxidation–reduction capacity of the catalysts[28].

As displayed in Fig. 4b, for all $Mn_yCe_{1-y}O_x$ catalysts, the Mn $2p_{3/2}$ XPS peaks can be divided into three peaks, of which 641.7 ± 0.1 eV and 642.5 ± 0.1 eV peaks represent Mn^{3+} and Mn^{4+}, respectively, while 644.5 ± 0.1 eV peak corresponds to the satellite peak of Mn[29–32]. The specific binding energy of Mn 2p is listed in Table 2. Compared with MnOx, the peak of Mn^{3+} and Mn^{4+} of $Mn_yCe_{1-y}O_x$ catalysts moves slightly to the lower binding energy. The deviation of the XPS peak indicates that the electron cloud densities of Mn^{3+} and Mn^{4+} of $Mn_yCe_{1-y}O_x$ catalysts are higher than those of MnO_x. It is due to the formation of Mn–O–Ce solid solution, which hinders the crystallization of MnO_x and causes lattice distortion. There are more defects on the surface of $Mn_yCe_{1-y}O_x$ catalysts than on the surface of MnO_x, which leads to the increase in electron cloud density of Mn^{4+}[33].

The Ce 3d spectra shown in Fig. 4c show complex overlapping peaks, which are decomposed into 8 peaks after peak separation fitting[15]. The details of these peaks are listed in Table 2. According to the peak area of Ce species, the proportion of Ce^{3+} ions in total Ce content is calculated[34], and the amount of Ce^{3+} is raised with the increase in Mn content. The proportion of Ce^{3+} in pure CeO_2 is 15.4%, while the $Mn_yCe_{1-y}O_x$ catalysts are 18.8%, 19.6%, 20.8%, and 22.1%, respectively. This means the proportion of Ce^{3+} increases slowly due to the formation of a small amount of weak Mn–O–Ce.

In conclusion, high relative contents of Mn^{4+} and Ce^{3+} ions usually reflect the excellent catalytic performances at low temperatures. The presence of Mn^{4+} ion is beneficial to improve the redox performance of the catalytic oxidation of 1,2-dichlorobenzene. The Ce^{3+} ion is generally considered to represent the oxygen vacancies of cerium-containing materials. As shown in Table 2, $Mn_{0.5}Ce_{0.5}O_x$ showed higher Mn^{4+} and Ce^{3+} ions content, and the relative contents of both $Mn^{4+}$and Ce^{3+} ions are shown a significant upward trend with the content of Mn.

Reducibility and surface acidity

As shown in Fig. 5a, the H_2-TPR profiles of pure MnO_x catalysts showed two overlapping strong reduction peaks. Under the assumption that MnO is the final reduced state, there are two reduction peaks for MnO_x catalysts at 490 °C and 590 °C, attributed to the reduction of $MnO_2 \rightarrow Mn_3O_4/Mn_2O_3$ and

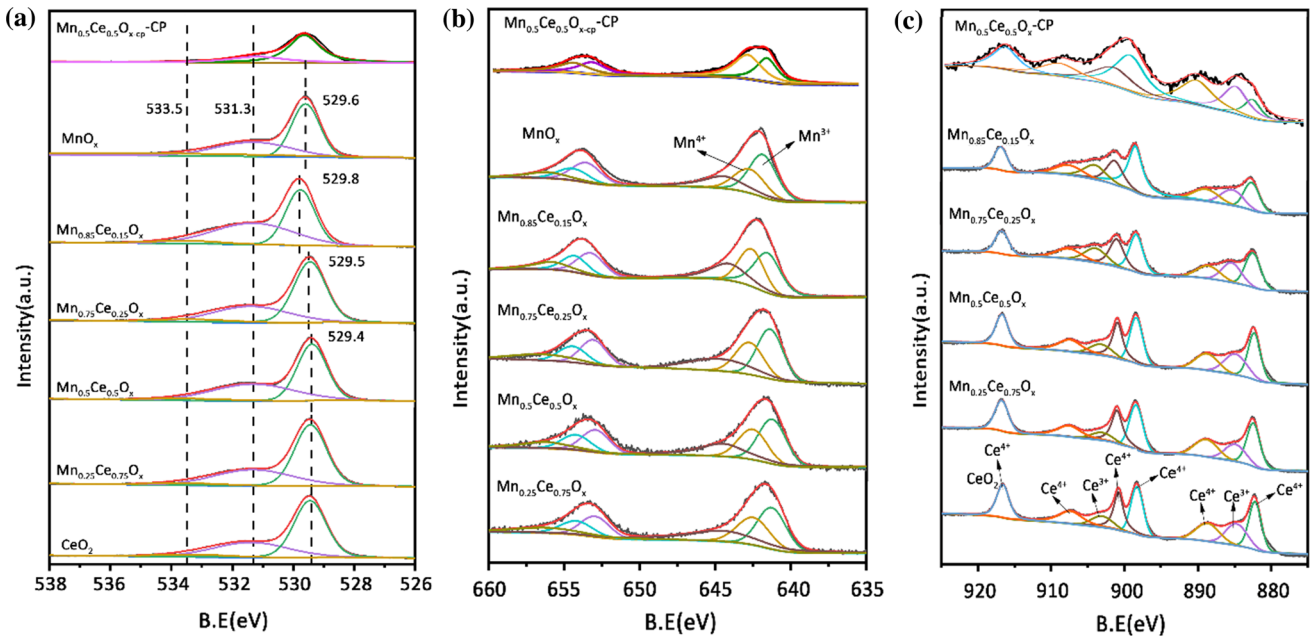

Figure 4 XPS spectra of **a** O 1 s, **b** Mn 2p, **c** Ce 3d for the $Mn_yCe_{1-y}O_x$ catalysts.

Table 2 Summary of the results of XPS analysis

Samples	Oxygen distribution(%)			Mn distribution (%)		Ce distribution (%)
	Olatt	Osur	Oads	Mn^{3+}	Mn^{4+}	Ce^{3+}
MnO_x	45	32.6	22.3	41.9	31.3	
$Mn_{0.85}Ce_{0.15}Ox$	46	48	6	43.3	30.3	22.1
$Mn_{0.75}Ce_{0.25}Ox$	47.5	46.7	5.8	41.2	29.6	20.8
$Mn_{0.5}Ce_{0.5}Ox$	52.5	42.2	5.2	36.4	28.8	19.6
$Mn_{0.25}Ce_{0.75}Ox$	58.7	36.5	4.9	45.7	27.1	18.8
CeO_2	63	30.9	6.1			15.4
$Mn_{0.5}Ce_{0.5}Ox$-CP	56.4	40.3	3.3	43.3	27.3	16.4

$Mn_3O_4/Mn_2O_3 \rightarrow MnO$, respectively[35–37]. However, the reduction of pure CeO_2 catalysts occurs in the temperature range of 300–500 °C, which is mainly related to the reduction of Ce^{4+} on the surface[27]. Compared with MnO_x and CeO_2 catalysts alone, the reduction characteristics of $Mn_yCe_{1-y}O_x$ mixed oxide catalysts generally show that the reduction temperature systematically shifts to a lower temperature region. The H_2-TPR profiles of $Mn_{0.25}Ce_{0.75}O_x$ catalysts with low Mn contents show two wide reduction peaks at 250 °C and 382 °C. The former may be related to the reduction of Mn^{4+} ions. The latter can be attributed to the reduction of Mn^{3+}, which is facilitated by high coordination unsaturation, perhaps by neighboring Ce^{4+}, which in turn is reduced to Ce^{3+}. For the $Mn_{0.5}Ce_{0.5}O_x$ catalysts, there is still an acromial peak at about 270 °C, indicating the presence of the isolated Mn^{4+}.Compared with $Mn_{0.5}Ce_{0.5}O_x$-CP, reduction peaks of $Mn_{0.5}Ce_{0.5}O_x$ were lower which proves that the catalytic reduction performance of $Mn_{0.5}Ce_{0.5}O_x$ was better than that of $Mn_{0.5}Ce_{0.5}O_x$-CP. When the ratio of Mn contents continues to increase, the $Mn_{0.75}Ce_{0.25}O_x$ catalysts first appear a reduction peak at the center of about 450 °C, which is related to the dispersion of very small MnO_2 particles on the Ce matrix in the first step of reduction. The second step of reduction occurs at a higher temperature of about 530 °C, which is caused by the gradual decrease in the number of Ce species. The first reduction peak of $Mn_{0.85}Ce_{0.15}O_x$ catalysts is significantly off-set to a lower temperature due to the formation of Mn–O-Ce solid solution, and the temperature of the second reduction peak is also initially decreased before the subsequent increase, which

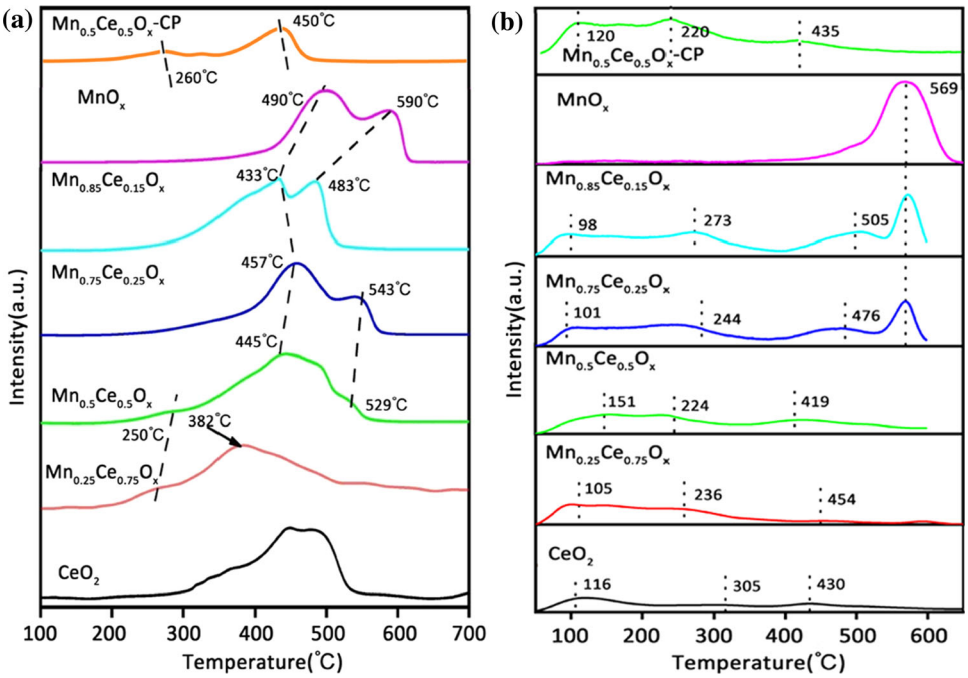

Figure 5 **a** H_2-TPR profiles of the $Mn_yCe_{1-y}O_x$ catalysts; **b** NH_3-TPD profiles of the $Mn_yCe_{1-y}O_x$ catalysts.

proves that the catalytic reduction performance of $Mn_{0.85}Ce_{0.15}O_x$ is the best. Therefore, for the $Mn_{0.5}Ce_{0.5}O_x$ catalysts with Mn/Ce = 1:1, the two reduction peaks are integrated into a wide peak cenetred at 450 °C, which may be related to the structural homogeneity caused by the formation of a large number of Mn–O–Ce solid solutions. In summary, there are two kinds of Mn^{4+} in the $Mn_yCe_{1-y}O_x$ catalysts, i.e., "isolated" Mn^{4+} and Mn^{4+}-O-Ce^{4+}; the latter mainly appears in the case of high Mn content ratio.

The surface acidity of each catalyst is evaluated by the NH_3-TPD experiment. According to Fig. 5b, the pure MnO_x catalysts do not appear an obvious desorption peak. However, at low temperatures, an overlapping NH_3 desorption peak is observed on both CeO_2 and $Mn_yCe_{1-y}O_x$ catalysts, indicating that the Ce species is mainly used to determine the surface acidity of the catalyst. The NH_3 species anchored on Brønsted acid sites (labeled as B acid) are less thermally stable than those adsorbed on Lewis acid sites (labeled as L acid)[38]. Consequently, the peaks at 100–200 °C in Fig. 5b are attributed to the desorption of ammonium ions (NH_4^+) weakly adsorbed on the B acid and those above 300 °C referring to the desorption of coordinate NH_3 on the L acid[39, 40]. It indicates that both L acid and B acid are required in the 1,2-DCBz catalytic oxidation, while the former is more effective in the reaction. Besides, many researchers claimed that the chemisorption of 1,2-DCBz through C–Cl cleavage occurs on the L acid preferentially[41, 42]. When Mn/(Mn + Ce) molar ratio is less than or equal to 0.5, the temperature of the desorption peaks observed on $Mn_yCe_{1-y}O_x$ catalysts is similar to that of CeO_2, indicating that the acid strength on the surface of these catalysts is similar. In contrast, when the Mn content continues to increase, the same peak as that of the pure MnO_x catalysts appears at 569 °C. However, the area of the three desorption peaks varies greatly among different catalysts. It is well known that peak area represents the total amount or number of acids on the catalyst surface. Through integral calculation, the order of peak area size of total NH_3-TPD is given by: $Mn_{0.85}Ce_{0.15}O_x$ > $Mn_{0.75}Ce_{0.25}O_x$ > MnO_x > $Mn_{0.5}Ce_{0.5}O_x$ > $Mn_{0.5}Ce_{0.5}O_x$-CP > $Mn_{0.25}Ce_{0.75}O_x$ > CeO_2. Therefore, $Mn_{0.5}Ce_{0.5}O_x$ have more acids on the catalyst surface than $Mn_{0.5}Ce_{0.5}O_x$-CP which further verified the superiority of ball-milling-assisted synthesis. And as compared with pure CeO_2 and MnO_x catalysts, the surface acidity of $Mn_yCe_{1-y}O_x$ mixed oxide catalysts is stronger, and the acidity of mixed oxide increases with the increase in Mn/Ce + Mn molar ratio.

Activity of $Mn_yCe_{1-y}O_x$ catalysts

As shown in Fig. 6, the catalytic activities of $MnCeO_x$ catalysts prepared by traditional co-precipitation

method (Mn/Ce = 1:1) are compared with the $MnCeO_x$ catalyst synthesized by the ball-milling-assisted method. The $Mn_{0.5}Ce_{0.5}O_x$-BM shows higher catalytic activity than the $Mn_{0.5}Ce_{0.5}O_x$-CP over the entire temperature range, achieving almost complete 1,2-DCBz conversion at 250 °C. In contrast, the $MnCeO_x$-CP only shows 60% conversion of 1,2-DCB_Z at the corresponding temperature. Catalytic combustion performance of 1,2-DCBz over $Mn_yCe_{1-y}O_x$ is also evaluated. According to Fig. 6b, T_{90} of 1,2-DCBz oxidation reaction decreased with the following order: $CeO_2 > MnO_x > Mn_{0.25}Ce_{0.75}O_x > Mn_{0.5}Ce_{0.5}O_x > Mn_{0.75}Ce_{0.25}O_x > Mn_{0.85}Ce_{0.15}Ox$, indicating that the best oxidation efficiency of 1,2-DCBz is above $Mn_{0.85}Ce_{0.15}O_x$ and the worst on CeO_2. For the $Mn_yCe_{1-y}O_x$ catalysts, except pure CeO_2, the removal efficiency of the other five catalysts for the catalytic oxidation of 1,2-dichlorobenzene is all improved with the increase in temperature. However, the removal efficiency of 1,2-dichlorobenzene catalyzed by CeO_2 decreases at 250 °C, and continues to rise when the temperature exceeds 350 °C, and the efficiency increases with temperature. The decrease in removal efficiency of 1,2-dichlorobenzene over CeO_2 catalyst at about 250 °C may be related to the chlorine poisoning of the catalyst. As discussed before, there is a strong interaction between Ce and Cl, and the catalysts containing Ce are seriously deactivated in the catalytic oxidation of chlorinated organic pollutants, and the activity of the catalysts continues to decrease

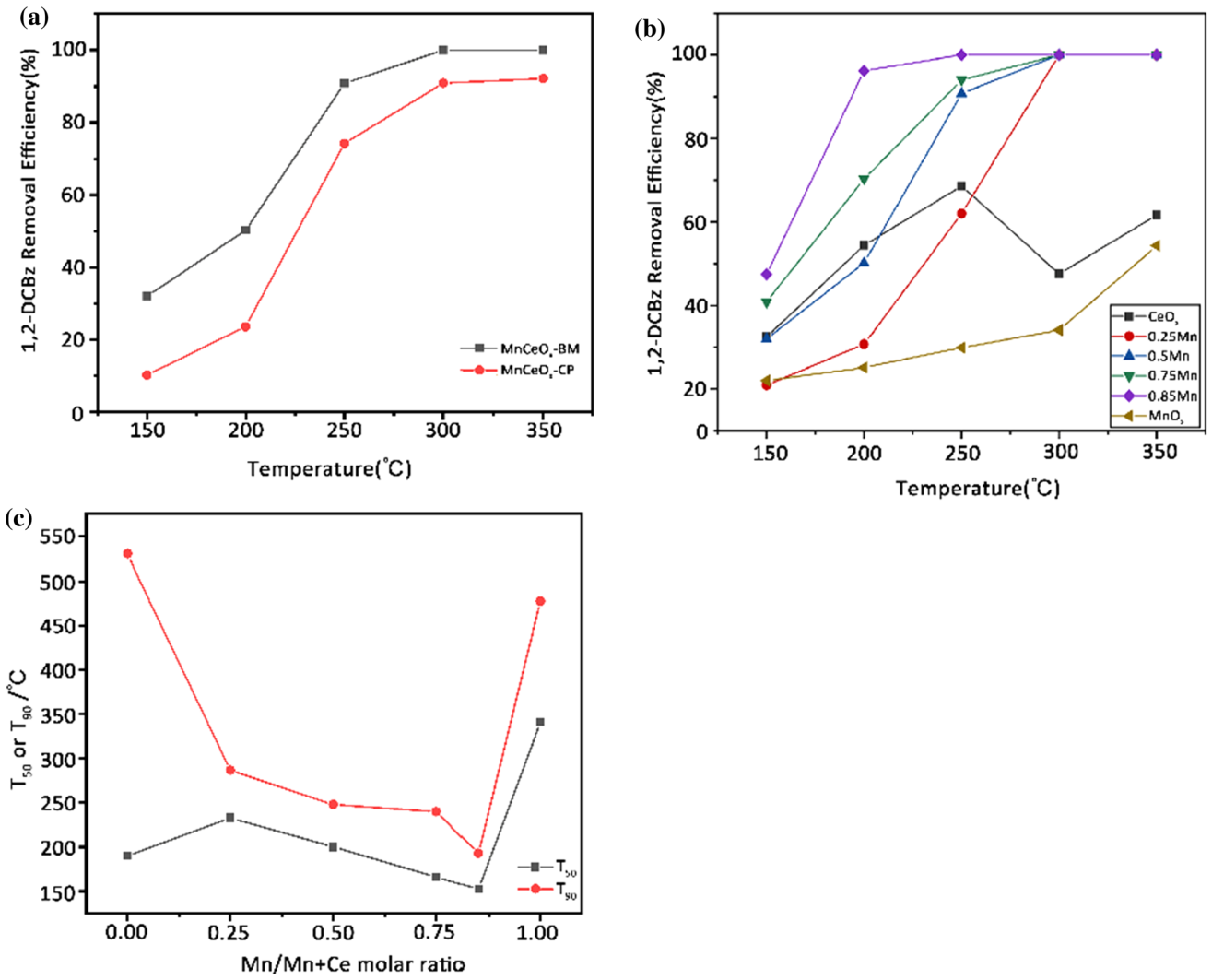

Figure 6 **a** The activity of $Mn_yCe_{1-y}O_x$ catalysts with different ratios of Mn/(Mn + Ce) for 1,2-DCBz catalytic combustion; **b** T_{90} and T_{50} for 1,2-DCBz combustion over $Mn_yCe_{1-y}O_x$ catalysts (gas composition: 200 ml/min,11% $O_2 + N_2$ balance; reactant concentration: 117 ppm; GHSV: 15,000 $h.^{-1}$; catalyst amount: 400 mg).

with the increase in reaction time. However, increasing the catalytic reaction temperature can enhance the Deacon reaction of Cl on the catalyst surface and accelerate the removal rate of Cl on the catalyst surface, thus reducing the degree of chlorine poisoning. Therefore, with the increase in reaction temperature, the removal efficiency of 1,2-dichlorobenzene catalyzed by CeO_2 increases.

$Mn_yCe_{1-y}O_x$ catalysts appear to be superior for 1,2-DCBz catalytic combustion, of which $Mn_{0.85}Ce_{0.15}O_x$ catalyst with 0.85 Mn/Mn + Ce ratio has the best activity, and the T_{90} of 1,2-DCBz oxidation reaction over the catalyst proceeds at about 193 °C, the temperature being much lower than all those catalysts as reported in previous literature, including Mn-modified Co3O4 catalyst[23] or CeO_2-TiO_2[42] and CeZn hollow microspheres catalysts[43]. As indicated by the characterization, the $Mn_{0.85}Ce_{0.15}O_x$ catalysts have the best surface structure, redox capacity, and acidity. The removal efficiency of 1,2-DCB_Z increases with the increase in Mn contents. As shown in Fig. 6, with the gradual increase in Mn/(Mn + Ce) molar ratio, T_{50} and T_{90} (the temperature needed for the conversion of 50% and 90%, respectively) gradually decrease, except the case of pure MnO_x. Over the pure MnO_x, the conversion of 1,2-DCBz reaches 90% at 478 °C, higher than that over the $Mn_yCe_{1-y}O_x$ catalysts. In conclusion, the addition of Mn increased the activity of Ce-based catalyst, and the degree of activity improvement is positively correlated with the ratio of Mn/(Mn + Ce).

Conclusion

In this work, we have successfully prepared a batch of Mn-Ce oxide catalysts with different molar ratios for the catalytic oxidation of 1,2-dichlorobenzene by the ball-milling-assisted solid-state synthesis. The ratio has a significant effect on the catalyst activity, and the degradation efficiency increases with the increase in Mn content. Complete removal is achieved at 193 °C when the ratio is 0.85, which is far better than the catalyst prepared by the co-precipitation method under the same conditions. This is mainly due to the high specific surface area and porosity of the catalyst synthesized by ball milling process, abundant active oxygen content, excellent acidity, reducibility and the formation of Mn–O–Ce chemical bond. The current work provides the potential to use the solvent-free large-scale ball-milling-assisted solid-state synthesis of low-temperature and high-activity catalysts in the field of environmental catalytic degradation.

Author contributions

Conceptualization: SL. Methodology: YG and SL. Data curation, formal analysis and investigation: YG, XG, JD. Writing—original draft preparation: YG. Writing—review and editing: YP. Funding acquisition: SL, YP. Resources: SL. Supervision: SL, and JY.

Funding

This work was supported by National Natural Science Foundation of China (51976192) and the China Postdoctoral Science Foundation funded project(2020M681851).

Availability of data and materials

Not applicable.

Declarations

Conflict of interest The authors declare no competing interests.

Ethical approval Not applicable.

Consent for publication Not applicable.

Consent to participate Not applicable.

References

[1] Taralunga M, Innocent B, Mijoin J, Magnoux P (2007) Catalytic combustion of benzofuran and of a benzofuran/1, 2-dichlorobenzene binary mixture over zeolite catalysts. Appl Catal B 75:139–146

[2] Aristizábal BH, Maya C, de Correa CM (2008) Ortho-dichlorobenzene oxidation over Pd/Co loaded sulfated zirconia and mordenite catalysts. Appl Catal A 335:211–219

[3] Choi J, Shin CB, Park T-J, Suh DJ (2006) Characteristics of vanadia–titania aerogel catalysts for oxidative destruction of 1, 2-dichlorobenzene. Appl Catal A 311:105–111

[4] Poplawski K, Lichtenberger J, Keil FJ, Schnitzlein K, Amiridis MD (2000) Catalytic oxidation of 1, 2-dichlorobenzene over ABO3-type perovskites. Catal Today 62:329–336

[5] Aristizabal BH, de Correa CM, Serykh AI, Hetrick CE, Amiridis MD (2008) In situ FTIR study of the adsorption and reaction of ortho-dichlorobenzene on Pd–Co sulfated zirconia catalysts. J Catal 258:95–102

[6] Yu M-F, Lin X-Q, Li X-D, Chen T, Yan J-H (2016) Catalytic decomposition of PCDD/Fs over nano-TiO2 based V2O5/CeO2 catalyst at low temperature. Aerosol Air Qualit Res 16:2011–2022

[7] De Rivas B, Guillén-Hurtado N, López-Fonseca R, Coloma-Pascual F, García-García A, Gutiérrez-Ortiz J, Bueno-López A (2012) Activity, selectivity and stability of praseodymium-doped CeO2 for chlorinated VOCs catalytic combustion. Appl Catal B 121:162–170

[8] Gu Y, Shao S, Sun W, Xia H, Gao X, Dai Q, Zhan W, Wang X (2019) The oxidation of chlorinated organic compounds over W-modified Pt/CeO2 catalysts. J Catal 380:375–386

[9] Gu Y, Cai T, Gao X, Xia H, Sun W, Zhao J, Dai Q, Wang X (2019) Catalytic combustion of chlorinated aromatics over WOx/CeO2 catalysts at low temperature. Appl Catal B 248:264–276

[10] Huang H, Gu Y, Zhao J, Wang X (2015) Catalytic combustion of chlorobenzene over VOx/CeO2 catalysts. J Catal 326:54–68

[11] Xingyi W, Qian K, Dao L (2009) Catalytic combustion of chlorobenzene over MnOx–CeO2 mixed oxide catalysts. Appl Catal B 86:166–175

[12] Li H, Wu S, Wu C-Y, Wang J, Li L, Shih K (2015) SCR atmosphere induced reduction of oxidized mercury over CuO–CeO2/TiO2 catalyst. Environ Sci Technol 49:7373–7379

[13] Lei Z, Hao S, Yang J, Zhang L, Fang B, Wei K, Lingbo Q, Jin S, Wei C (2021) Study on denitration and sulfur removal performance of Mn–Ce supported fly ash catalyst. Chemosphere 270:128646

[14] Sun Z, Wang J, Zhu J, Wang C, Wang J, Shen M (2017) Investigation of the active sites for NO oxidation reactions over MnO x–CeO 2 catalysts. New J Chem 41:3106–3111

[15] Shao J, Lin F, Li Y, Tang H, Wang Z, Liu P, Chen G (2019) Co-precipitation synthesized MnOx-CeO2 mixed oxides for NO oxidation and enhanced resistance to low concentration of SO2 by metal addition. Catalysts 9:519

[16] Meng X, Bi X, Yu C, Chen G, Chen B, Jing Z, Zhao P (2018) Ball-milling synthesized hydrotalcite supported Cu–Mn mixed oxide under solvent-free conditions: an active catalyst for aerobic oxidative synthesis of 2-acylbenzothiazoles and quinoxalines. Green Chem 20:4638–4644

[17] Cheng H, Tan J, Ren Y, Zhao M, Liu J, Wang H, Liu J, Zhao Z (2019) Ball milling synthesis of highly porous CeMnO x catalyst for the removal of NO x. Ind Eng Chem Res 58:16472–16478

[18] Gan L, Li K, Niu H, Peng Y, Chen J, Huang Y, Li J (2021) Simultaneous removal of NO x and chlorobenzene on V 2 O 5/TiO 2 granular catalyst: Kinetic study and performance prediction. Front Environ Sci Eng 15:1–10

[19] Gao C, Yang G, Huang X, Yang Q, Li B, Wang D, Peng Y, Li J, Lu C, Crittenden J (2021) Key intermediates from simultaneous removal of NO x and chlorobenzene over a V2O5–WO3/TiO2 catalyst: a combined experimental and DFT study, catalysis. Sci Technol 11:7260–7267

[20] Gan L, Shi W, Li K, Chen J, Peng Y, Li J (2018) Synergistic promotion effect between NOx and chlorobenzene removal on MnOx–CeO2 Catalyst. ACS Appl Mater Interfaces 10:30426–30432

[21] Zhang Q, Ariga K, Okabe A, Aida T (2004) A condensable amphiphile with a cleavable tail as a “lizard” template for the sol− gel synthesis of functionalized mesoporous silica. J Am Chem Soc 126:988–989

[22] Machida M, Uto M, Kurogi D, Kijima T (2000) MnOx−CeO2 binary oxides for catalytic NOx sorption at low temperatures. Sorptive removal of NOx. Chem Mater 12:3158–3164

[23] Cai T, Huang H, Deng W, Dai Q, Liu W, Wang X (2015) Catalytic combustion of 1, 2-dichlorobenzene at low temperature over Mn-modified Co3O4 catalysts. Appl Catal B 166:393–405

[24] Chen L, Liu G, Feng N, Yu J, Meng J, Fang F, Zhao P, Wang L, Wan H, Guan G (2019) Effect of calcination temperature on structural properties and catalytic soot combustion activity of MnOx/wire-mesh monoliths. Appl Surf Sci 467:1088–1103

[25] López JM, Gilbank AL, García T, Solsona B, Agouram S, Torrente-Murciano L (2015) The prevalence of surface oxygen vacancies over the mobility of bulk oxygen in nanostructured ceria for the total toluene oxidation. Appl Catal B 174:403–412

[26] Martínez-Arias A, Fernández-García M, Belver C, Conesa J, Soria J (2000) EPR study on oxygen handling properties of ceria, zirconia and Zr–Ce (1: 1) mixed oxide samples. Catal Lett 65:197–204

[27] Arena F, Trunfio G, Negro J, Fazio B, Spadaro L (2007) Basic evidence of the molecular dispersion of MnCeO x catalysts synthesized via a novel “redox-precipitation” route. Chem Mater 19:2269–2276

[28] Du C, Wang Q, Peng Y, Lu S, Ji L, Ni M (2017) Catalytic oxidation of 1, 2-DCBz over V 2 O 5/TiO 2-CNTs: effect of

CNT diameter and surface functional groups. Environ Sci Pollut Res 24:4894–4901

[29] Meng D, Zhan W, Guo Y, Guo Y, Wang L, Lu G (2015) A highly effective catalyst of Sm-MnO x for the NH3-SCR of NO x at low temperature: promotional role of Sm and its catalytic performance. ACS Catal 5:5973–5983

[30] Yang S, Xiong S, Liao Y, Xiao X, Qi F, Peng Y, Fu Y, Shan W, Li J (2014) Mechanism of N2O formation during the low-temperature selective catalytic reduction of NO with NH3 over Mn–Fe spinel. Environ Sci Technol 48:10354–10362

[31] Yang Y, Zhang S, Wang S, Zhang K, Wang H, Huang J, Deng S, Wang B, Wang Y, Yu G (2015) Ball milling synthesized MnO x as highly active catalyst for gaseous POPs removal: significance of mechanochemically induced oxygen vacancies. Environ Sci Technol 49:4473–4480

[32] Chen J, Shen M, Wang X, Qi G, Wang J, Li W (2013) The influence of nonstoichiometry on LaMnO3 perovskite for catalytic NO oxidation. Appl Catal B 134:251–257

[33] Liu H, Li X, Dai Q, Zhao H, Chai G, Guo Y, Guo Y, Wang L, Zhan W (2021) Catalytic oxidation of chlorinated volatile organic compounds over Mn-Ti composite oxides catalysts: elucidating the influence of surface acidity. Appl Catal B 282:119577

[34] Zou Z-Q, Meng M, Zha Y-Q (2010) Surfactant-assisted synthesis, characterizations, and catalytic oxidation mechanisms of the mesoporous MnOx− CeO2 and Pd/MnOx−CeO2 Catalysts Used for CO and C3H8 oxidation. J Phys Chem C 114:468–477

[35] Kapteijn F, Singoredjo L, Andreini A, Moulijn J (1994) Activity and selectivity of pure manganese oxides in the selective catalytic reduction of nitric oxide with ammonia. Appl Catal B 3:173–189

[36] Arena F, Trunfio G, Negro J, Spadaro L (2008) Optimization of the MnCeOx system for the catalytic wet oxidation of phenol with oxygen (CWAO). Appl Catal B 85:40–47

[37] Ferrandon M, Carnö J, Järås S, Björnbom E (1999) Total oxidation catalysts based on manganese or copper oxides and platinum or palladium I: characterisation. Appl Catal A 180:141–151

[38] Hussain ST, Sayari A, Larachi FÇ (2001) Enhancing the stability of Mn–Ce–O WETOX catalysts using potassium. Appl Catal B Environ 34:1–9

[39] Li Y, Wan Y, Li Y, Zhan S, Guan Q, Tian Y (2016) Low-temperature selective catalytic reduction of NO with NH3 over Mn2O3-doped Fe2O3 hexagonal microsheets. ACS Appl Mater Interfaces 8:5224–5233

[40] Anstrom M, Topsøe N-Y, Dumesic J (2003) Density functional theory studies of mechanistic aspects of the SCR reaction on vanadium oxide catalysts. J Catal 213:115–125

[41] Boningari T, Ettireddy PR, Somogyvari A, Liu Y, Vorontsov A, McDonald CA, Smirniotis PG (2015) Influence of elevated surface texture hydrated titania on Ce-doped Mn/TiO2 catalysts for the low-temperature SCR of NOx under oxygen-rich conditions. J Catal 325:145–155

[42] Wu M, Wang X, Dai Q, Gu Y, Li D (2010) Low temperature catalytic combustion of chlorobenzene over Mn–Ce–O/γ-Al2O3 mixed oxides catalyst. Catal Today 158:336–342

[43] Deng W, Dai Q, Lao Y, Shi B, Wang X (2016) Low temperature catalytic combustion of 1, 2-dichlorobenzene over CeO2–TiO2 mixed oxide catalysts. Appl Catal B 181:848–861